RSC Advances

PAPER

View Article Online
View Journal | View Issue

Cite this: *RSC Adv.*, 2025, **15**, 28881

Photo-driven color-conversion display based on a thermochromic-liquid-crystal and carbon-nanotube film

Taekyung Lim, Sang-Mi Jeong, Hee Sung Seo, Jonguk Yang* and Sanghyun Ju *

Light-irradiation-based color-conversion displays are considered an emerging technology with considerable potential because they are easy to fabricate; however, color precision is limited by inefficient heating and uneven temperature distribution, and pattern extinction is delayed by poor heat dissipation. This study proposes a light-irradiation-based color-conversion display that can produce full color from a near-infrared (NIR) laser using carbon nanotubes (CNTs) with efficient photothermal conversion and heat-diffusion functions. Light-irradiation-based color-conversion displays have a more straightforward structure than conventional electronic-circuit-based displays. The proposed design uses an NIR laser as the driving energy source, which makes it highly efficient. In addition, a color-conversion layer based on a thermochromic liquid crystal (TLC) changes the color to red, green, or blue depending on the temperature, and a CNT-based thermal property control layer, which reacts to NIR photothermally, is used to achieve immediate thermal control. These layers can be applied to a flexible substrate to maintain stable performance, even under bending or deformation. Precisely controlling the laser power can help achieve a subtle temperature change of 27–32 °C and generate a corresponding color change in a specific area of the TLC-based color-conversion layer. Considering rapid and reversible color conversion is achievable by turning the NIR laser on and off, this method is suitable for various applications, such as high-speed responsive displays, smart sensors, and customizable visual information systems.

Received 4th April 2025
Accepted 9th August 2025

DOI: 10.1039/d5ra02339d

rsc.li/rsc-advances

Introduction

Display technology is a key element of information transmission and interaction in modern society. The mainstream display technologies currently include liquid crystal displays (LCDs), organic light-emitting diodes (OLEDs), and micro light-emitting diodes (micro-LEDs). Most of these are active-matrix-based pixel-driving displays, which require individually controllable pixels and electronic circuits to operate.[1,2] The pixels form linear circuits, which are crucial for achieving high resolution, brightness uniformity, and accurate gray-scale representation in displays. However, due to the presence of numerous thin-film transistors (TFTs) that constitute these circuits, the complexity of the circuits and fabrication processes increases. Additionally, compensation for manufacturing variations and the aging of device characteristics for each TFT is required.[3] Therefore, for the development of next-generation displays, there is growing interest in TFT-free displays that do not require complex and costly electronic circuits, such as TFT fabrication, and can be fabricated more easily. In contrast to active-matrix-based pixel-driving displays, light-irradiation-based color-conversion displays are simple and efficient to produce.[4,5] They induce color conversion by irradiating materials with light of a specific wavelength, which does not require electrical driving. Therefore, they have a simple structure and offer high energy efficiency compared with existing displays. In addition, light-irradiation-based color-conversion displays can be applied to flexible substrates, which endows them with mechanical properties such as elasticity and helps them maintain stable performance even when bent or deformed. Owing to these characteristics, this technology may be used to develop displays that change color according to external environmental changes, such as smart windows, temperature-sensitive sensors, wearable displays, and head-up displays, or displays that only show information under certain conditions.[6–9] Moreover, more innovative applications may be developed by merging next-generation interfaces and sensor technologies.[10–12]

Thermochromic liquid crystals (TLCs), *i.e.*, organic compounds that change color at specific temperatures, mainly exist as cholesteric liquid crystals, which form a spiral arrangement. The spiral pitch is affected by the temperature, which changes the wavelength of the reflected light owing to Bragg's reflection, thereby changing the observed color.[13] When

Major in Nano Semiconductor, School of Electronic Engineering, Kyonggi University, Suwon, Gyeonggi-do 16227, Republic of Korea. E-mail: juyang@kgu.ac.kr; shju@kgu.ac.kr

the temperature increases, the pitch decreases and shorter wavelengths are reflected. By contrast, when the temperature decreases, the pitch increases and longer wavelengths are reflected.[14] Microencapsulation technology, which improves the stability of these color changes, can be used to protect TLCs from the external environment. The polymer coatings used for microencapsulation also increase the durability of the TLCs and protect them from external impact or chemical damage.[15] Moreover, TLCs are composed of organic molecules, such as cholesterol or biphenyl derivatives, which are highly hydrophobic, durable, and can be used to coat various substrates. Therefore, TLCs can be applied to various materials, such as flexible films, glass, and plastics, thus highlighting their practicality for many applications.[16,17]

TLC films are easy to fabricate, and their colors can be precisely controlled by inducing localized heating using infrared lasers, which have high penetrability and energy density. Thus, the temperature of a specific area can be controlled to form various color patterns.[18] TLCs also exhibit excellent durability and are not easily damaged by infrared laser irradiation. Therefore, they can maintain stable color changes during repeated heating and cooling processes, thus highlighting their reusability. However, the precision of color implementation may be reduced by poor heating efficiency and non-uniform temperature distribution, and the rate at which a specific pattern can disappear is limited. Therefore, research is required to develop efficient technologies that can control heating and heat dispersion to maintain a uniform temperature distribution.

In this study, we aim to address the pattern extinction delay problem by improving the heat-dispersion efficiency—achieved by applying carbon nanotubes (CNTs) to a TLC film to form a carbon nanotube–styrene–ethylene–butylene–styrene (CNT–SEBS) photothermal film (used as a color-conversion layer). CNTs have excellent thermal conductivity (~6600 W m^{-1} K^{-1}) and high light absorption, and their high absorption rate in the near-infrared region is particularly suitable for inducing the photothermal effect.[19,20] The excellent photothermal conversion performance of the CNTs was utilized to improve the heat-generation characteristics, which facilitated red/green/blue (RGB) color implementation and precise color pattern control, thus addressing the limitations of existing TLC films. In addition, the improved heat generation and heat release characteristics of the CNT-based TLC film enabled fast and precise generation of full-color images. Therefore, the proposed method offers considerable potential for various applications such as high-speed responsive displays, smart sensors, and personalized visual information systems and is expected to lead to the development of next-generation display technology.

Experimental details

Fabrication of a color-conversion display with a CNT–SEBS photothermal film based on light irradiation

Uniform mixing of the CNTs (MR99, Carbon Nano-material Technology) and polymers was ensured by polarizing the surfaces of the CNTs by subjecting them to ultraviolet-ozone treatment (UVO Cleaner, AhTECH Leading Technology Systems Co.) for 1 h. Varying amounts of the treated CNTs were added to 50 g of cyclopentyl methyl ether (CPME; Sigma Aldrich) and dispersed by ultrasonication (LK-U225D, SD-Ultra) for 1 h. Subsequently, 10 g of styrene ethylene–butylene styrene (SEBS, KRATON Corp.) was added to the dispersed solution, and the mixture was mixed using a paste mixer (400-DI, LM-Tech) at 800 rpm. The CNT content was 1–10 wt% relative to the SEBS content. After mixing, the solution was cast onto a 300 × 300 mm glass plate and allowed to dry naturally at room temperature (~25 °C) for approximately 30 min. The CNT–SEBS film was dried in an oven at 90 °C for approximately 12 h to completely volatilize the remaining solvent. After drying, the CNT–SEBS film was molded into a CNT–SEBS photothermal film with a uniform thickness of approximately 270 μm using a hot press (QM900L, Qmesys) at a temperature of 170 °C and a pressure of 400 kg cm^{-2}. One surface of the photothermal film was spin-coated with liquid crystal ink (SFXC) at 1000 rpm for 30 s, and the sample was cut to 70 × 70 mm. Subsequently, the mixture was dried in an oven at 60 °C for 30 min. The TLC layer on the manufactured display was measured to be approximately 50 μm thick.

Characteristics of color-conversion display using light irradiation

The thermal conductivities of the CNT–SEBS photothermal films with different CNT contents were measured using Hot Disk (TPS 2500S, Hot Disk®). A 70 × 70 mm specimen was attached above and below the thermal conductivity measurement sensor (5465 F2, Kapton-insulated Sensors) and pressed to flatten it before measurement. The measurement time per specimen was 10 s, the measurements were repeated three to five times, and the heating power was 20 mW.

The mechanical properties of the CNT–SEBS films were measured by rheometer (Discovery HR20, TA Instruments). The specimen length was increased to 5000 μm at a rate of 200 μm min^{-1}, and the strain corresponding to the increased tensile load was measured to obtain a stress–strain curve. Thermogravimetric analysis (TGA, Hitachi High-Tech Analytical Science Co., Ltd) was used to analyze the CNT content of the CNT–SEBS photothermal films. The samples were heated to 600 °C at a rate of 20 °C min^{-1} and cooled at a rate of 10 °C min^{-1}. The TGA showed that the mass of the samples changed as the temperature increased to 600 °C.

Driving color-conversion display using light irradiation

A 1064 nm near-infrared (NIR) laser marking machine (Mini1064-30, Changchun New Industries Optoelectronics Tech. Co., Ltd) with a spot size of ~50–100 μm was used to induce local photothermal reactions on the CNT–SEBS film. The image scanned by the laser was designed using the EzCad2 software (ver. 2.99; Beijing JCZ Technology Co., Ltd). For smooth temperature control, an NIR-absorbing film (CR20, 3M, Minnesota, USA) was installed as a damper between the NIR laser and color-conversion display substrate (the distance between the color-conversion display substrate and damper was

35 mm). The color was controlled by adjusting the power of the NIR laser to 14–38% (power 20–56 mW; power density 2.037–5.704 kW cm^{-2}). The speed and frequency were fixed at 100 mm s^{-1} and 70 kHz, respectively. An infrared camera (T420, FLIR® Systems, Inc., Oregon, USA) was used to confirm the temperature of the irradiated substrate and obtain infrared images. The images of the shapes formed on the window display were analyzed using the open-source video analysis and modeling tool Tracker (**http://physlets.org/tracker/**) to extract the luminance values for each color R, G, and B. For the temperature and color analysis of the line, values at five points were extracted and averaged.

Results and discussion

Fig. 1(a) shows a schematic of a TLC, the color-conversion material used for the light-irradiation-based color-conversion display. The TLCs used in this study were translucent cholesteric liquid crystals encapsulated with a maximum size of ~12 μm. In the TLC cholesteric phase, each molecular layer is rotated and stacked at a certain angle according to its orientational order. The cholesteric phase can exhibit different reflection/transmission intensities depending on the helical structure and polarization of the incident light. For example, light is reflected in the same direction as the helical structure and not in the opposite direction. In the case of unpolarized incident light, up to 50% of the incoming light can be reflected.[21,22]

The Bragg reflection wavelength λ of the helical structure is dependent on the helical pitch of the cholesteric phase. Previous analysis of the thermodynamic vibrations near the cholesteric-smectic A* phase transition has shown that the helical pitch of the cholesteric phase is inversely proportional to the temperature.[23,24] Therefore, the color reflected in the visible light region can be controlled using the temperature of the TLC. Fig. 1(b) shows the color of the TLC material according to the temperature of the color-conversion display substrate, which was determined using an optical microscope. As the temperature increased, the color of the encapsulated cholesteric liquid crystal gradually changed from black (<25 °C) to red (27 °C), green (29 °C), and blue (32 °C). At temperatures below 25 °C, the pristine TLC was initially translucent; however, it appeared black owing to the underlying CNT–SEBS.

Fig. 1(c) illustrates the operation of a color-conversion display based on light irradiation using a NIR laser. A substrate that generates a photothermal reaction is required to fabricate a color-conversion display based on light irradiation using an NIR laser. CNTs generate heat rapidly when they are irradiated with an NIR laser owing to their high light absorption rate, and they cool quickly owing to their high thermal conductivity. Therefore, they have the characteristics required to control the color of the TLC using heat. The CNTs were composited with a highly elastic SEBS polymer to form a flexible film. When an NIR laser with a wavelength of 1064 nm irradiated the CNT–SEBS photothermal film in the color-conversion display substrate, the CNTs absorbed the NIR irradiation and rapidly released heat through an exothermic photothermal reaction. The heat released from the CNT–SEBS film was transferred to the TLC coating, which changed the helical pitch of the liquid crystal structure. As the temperature of the TLC coating increased, the helical pitch became shorter and the reflected light was blue-shifted. Therefore, by precisely

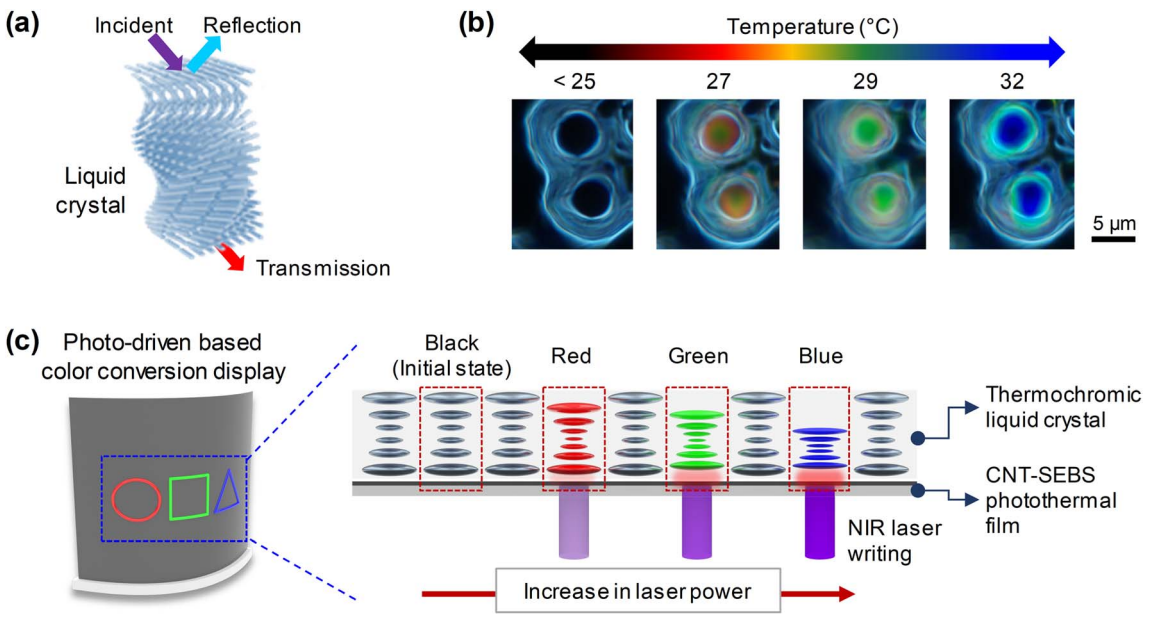

Fig. 1 Implementation of a color-conversion display based on light irradiation. (a) Schematic showing the structure of the thermochromic liquid crystals (TLCs). (b) Photographs showing the temperature-related color change. (c) Schematic showing the operation of a color-conversion display based on light irradiation with a near-infrared (NIR) laser writing on a substrate composed of TLC and carbon nanotube–styrene–ethylene–butylene–styrene (CNT–SEBS).

controlling the temperature of the TLC coating through NIR laser irradiation, red, green, and blue colors could be expressed. In addition, when the NIR laser was turned off, the TLC coating cooled quickly owing to the high heat dissipation characteristics of the CNTs, and the color of the TLC returned to its original state. Therefore, a color-conversion display based on light irradiation can be achieved by utilizing the photothermal and heat dissipation characteristics of CNTs.

The thermal characteristics of the CNT–SEBS films were investigated using TGA, as shown in Fig. 2(a). The thermal decomposition characteristics between 0 and 600 °C showed that mass loss occurred at temperatures above 300 °C—a recognized thermal decomposition characteristic of polymers[25] and can be considered as the start of SEBS decomposition. The SEBS film (0 wt% CNTs) decomposed completely and was converted to CO_2 at approximately 420 °C, and the residue at 600 °C was 1.5% of the original weight. The CNT–SEBS films showed the same thermal decomposition results as the SEBS film, starting at approximately 300 °C and saturating at approximately 420 °C. Owing to their high thermal stability, the CNTs did not decompose, even at 600 °C, and remained in the residue. As the CNT content increased, the weight of the residue at 600 °C gradually increased, and the weights of the residues at CNT contents of 1, 2, 4, 6, 8, and 10 wt% were 1.9%, 2.4%, 3.1%, 4.7%, 5.5%, and 7.2%, respectively. The thermal conductivity, which represents the heat dissipation ability, of the SEBS film (0 wt% CNTs) was 675 ± 2.8 mW m^{-1} K^{-1}, which increased to 689 ± 2.4 and 1048 ± 18.3 mW m^{-1} K^{-1} as the CNT content increased from 1 to 10 wt%, as shown in Fig. 2(b).

Fig. 2(c) shows the photothermal response characteristics when an NIR laser was applied to the CNT–SEBS films (0–10 wt% CNTs). The NIR laser was turned on at a power of 51 mW after 5 s, held at that power for 90 s, and then turned off. In the case of the SEBS film (0 wt% CNTs), the temperature remained approximately constant, even when the laser was applied, as there was no light-absorbing medium. By contrast, the temperatures of the CNT–SEBS films increased rapidly as soon as the laser was applied. The response time for the temperature increase after the laser was applied was ~10 s, and the CNT content had no significant effect. By contrast, the cooling time after the laser was turned off decreased from 12.4 to 9.0 s as the CNT content increased from 1 to 10 wt%.

The response and decay times were calculated using the equations

$$I_{\text{response}}(t) = I_0 + A_1(1 - e^{(-t/\tau_r)}) \quad (1)$$

and

$$I_{\text{decay}}(t) = I_0 + A_2(e^{(-t/\tau_d)}), \quad (2)$$

where I_0 is the initial value, τ_r is the response time constant, τ_d is the decay time constant, and A_1 and A_2 are constants.

The temperature at 95 s, just before the laser was turned off, gradually decreased as the CNT content increased and saturation occurred when the CNT content was 8 wt%. The temperatures at 95 s for the films with CNT contents of 1, 2, 4, 6, 8, and 10 wt% were 32.3, 32.0, 31.6, 31.3, 30.9, and 30.7 °C, respectively, because the thermal conductivity of the film increased as

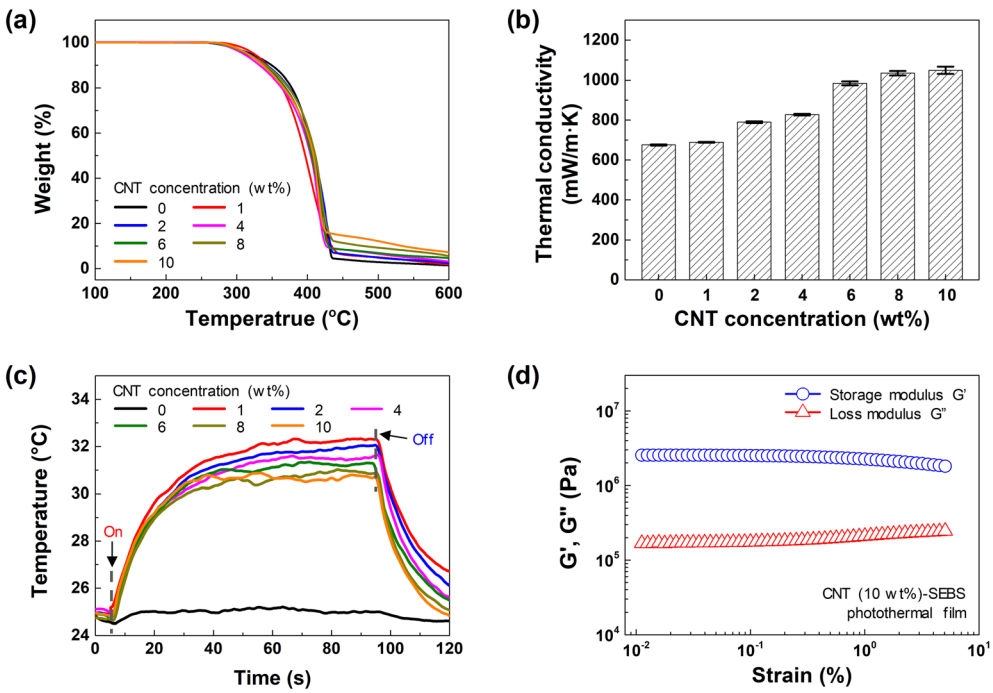

Fig. 2 Characterization of the CNT–SEBS film. (a) Thermogravimetric analysis (TGA) of the CNT–SEBS films with different CNT contents (0–10 wt%) between 100 and 600 °C. (b) Thermal conductivity of the films. (c) Heating/cooling characteristics of the films during laser irradiation. (d) Dynamic viscoelastic measurement results of the CNT (10 wt%)–SEBS photothermal film.

the CNT content increased, which reduced the amount of heat accumulation. Based on these results, a CNT–SEBS photothermal film with a CNT content of 10 wt% was used as the substrate for the light-irradiation-based color-conversion display. Fig. 2(d) shows the results of elastic analysis conducted using a rheometer to confirm the high elasticity of the CNT–SEBS film. From the dynamic viscoelastic results, the tensile storage (elastic) modulus E' and the tensile loss (viscous) modulus E'' of the polymer solid could be obtained through bending, rod torsion, and simple elongation, and the storage modulus G' and the loss modulus G'' could be determined. A higher G' indicates stronger elastic properties, while a higher G'' indicates dominant viscosity. The ratio of viscoelasticity can be identified by tan δ.[26]

$$\tan\ \delta = \frac{G''}{G'}$$

In general, when $\tan\delta \ll 1$, it indicates that the material is highly elastic.[27] The tan δ of the CNT (10 wt%)–SEBS photothermal film was 0.066, and the tan δ of the SEBS film was 0.057. Due to the reinforcing effect resulting from the presence of CNT inside SEBS, the force required for deformation was increased,[28] but a tan δ below 0.1 indicates that it was sufficiently highly elastic.

Heat was transferred from the CNT–SEBS photothermal film to the TLC layer through an exothermic photothermal reaction that occurred when the CNTs absorbed the NIR light when they were irradiated by the laser. Moreover, the heat was rapidly removed from the TLC layer by the CNT–SEBS photothermal film when the NIR laser was turned off. As shown in Fig. 3(a), the surface temperature of the TLC layer increased as the laser power increased. The surface temperature of the TLC layer remained constant for approximately 30 s after laser irradiation. After 30 s, the surface temperatures under laser powers of 20, 25, 31, 36, 39, and 56 mW were 26.2, 27.3, 27.9, 29.5, 30.4, and 32.0 °C, respectively. Thus, 25, 36, and 56 mW were selected as the laser powers that matched the RGB color change temperatures of the TLC layer at 27 °C (red), 29 °C (green), and 32 °C (blue). As shown in Fig. 3(b), the surface temperature of the TLC layer could be changed rapidly and maintained by the optimized NIR laser irradiation, and it returned to its original state within 20 s when the NIR laser was turned off. These results show that RGB color changes can be generated in specific areas of the display substrate using an NIR laser, which enables the formation of various full-color images.

Fig. 3(c) shows infrared and visible images of the surface temperature and color changes of the light-irradiation-based color-conversion display irradiated with different laser powers in a line shape with a length of 30 mm. As the energy of the laser increased, the temperature generated in the CNT–SEBS photothermal film increased, which transferred more heat to the TLC layer. When the CNT–SEBS photothermal film was irradiated by the NIR laser, the CNTs rapidly absorbed the NIR radiation, which initiated the exothermic reaction. As shown in Fig. 3(c), when the laser power was low (16 mW), the TLC did not reach the color-conversion temperature and no color conversion was observed in the visible images. However, when the power was

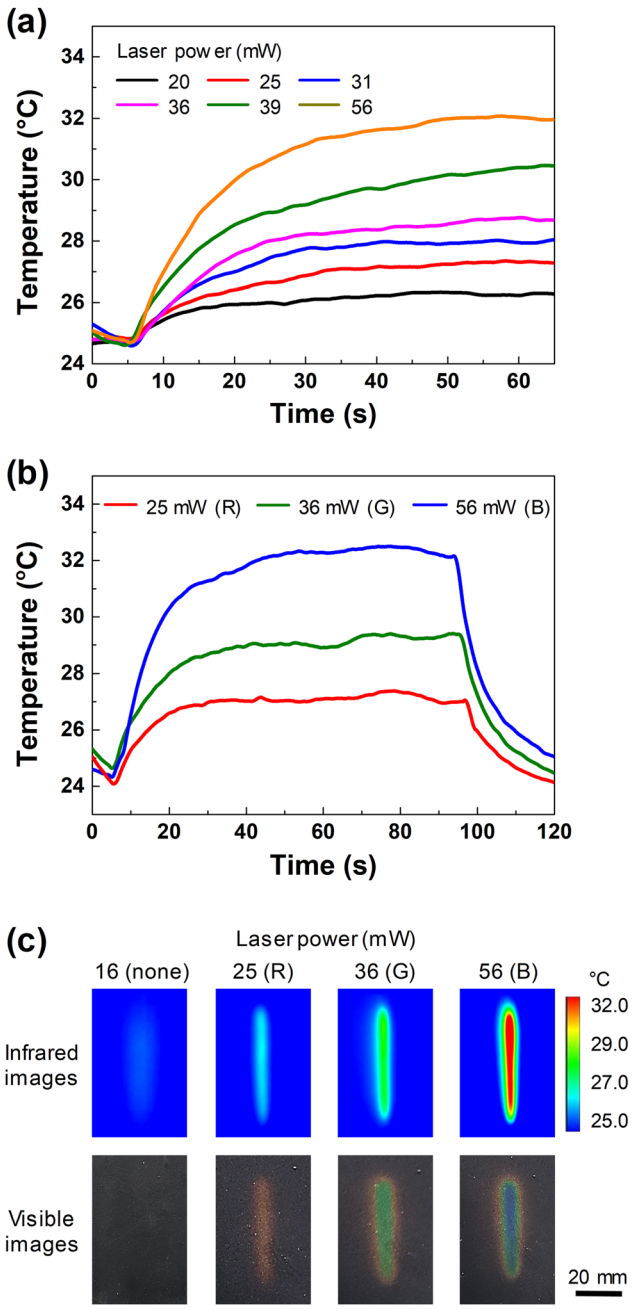

Fig. 3 Heat-generation characteristics of a color-conversion display with different NIR laser irradiation conditions. (a) Surface temperature of the display at different laser powers (20, 25, 31, 36, 39, and 56 mW). (b) RGB color expression of the display (R/G/B = 25/36/56 mW). (c) Infrared and visible images showing the surface temperature and color change of the TLC layer at different NIR laser powers.

increased to 25 mW or more, the temperature at the center of the irradiated region increased, which was confirmed by the infrared image. When the laser powers were 16, 25, 36, and 56 mW, the surface temperatures of the lines were 25.6 ± 0.1, 26.9 ± 0.15, 28.7 ± 0.38, and 31.5 ± 0.8 °C, respectively, and the corresponding TLC color-conversion layer colors were black (RGB color values of 51 ± 6.4, 52.2 ± 6.7, and 55.6 ± 6.4), red (115 ± 4.2, 83.8 ± 2.6, and 73 ± 4.6), green (75 ± 4.4, 123.8 ±

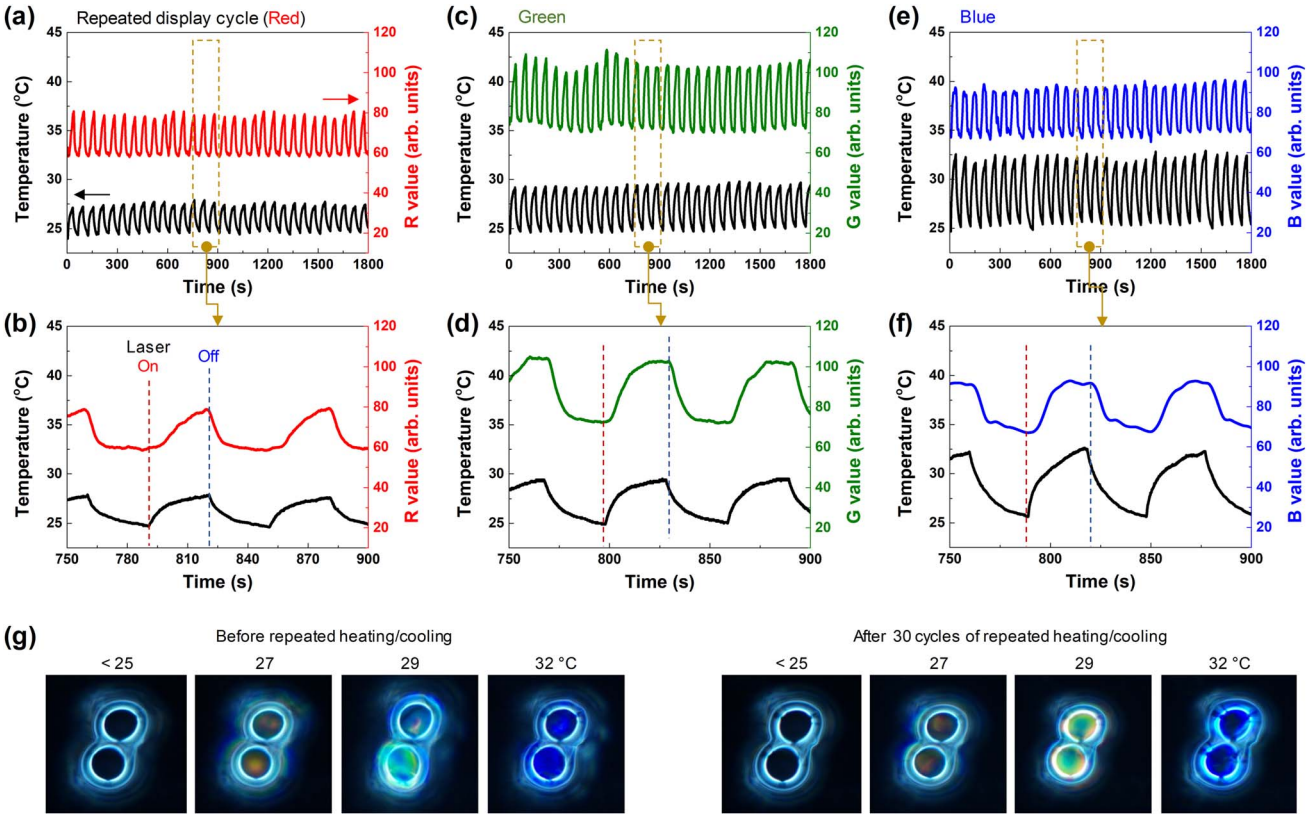

Fig. 4 Repeated RGB color generation by the light-irradiation-based color-conversion display. The on/off time for all the displays was fixed at 30/30 s. Repeated driving characteristics of the (a and b) red (laser power: 25 mW), (c and d) green (laser power: 36 mW), and (e and f) blue (laser power: 56 mW) displays. (g) Optical microscope image of the TLC capsule after 30 cycles of repeated heating/cooling (5/5 min) testing.

7.6, and 83.4 ± 7.8), and blue (63 ± 1.9, 88.2 ± 5.8, and 117.2 ± 7.5), respectively.

For practical applications, the light-irradiation-based color-conversion display must reliably reproduce color expression. Therefore, to ensure the reliability of the color expression of the fabricated display, the color-conversion process from the black initial state to the red, green, and blue states under different NIR laser driving conditions was measured repeatedly. The NIR laser powers optimized for the RGB color expression of the TLC (Fig. 3(b)) were 25 (red), 36 (green), and 56 (blue) mW. The on/

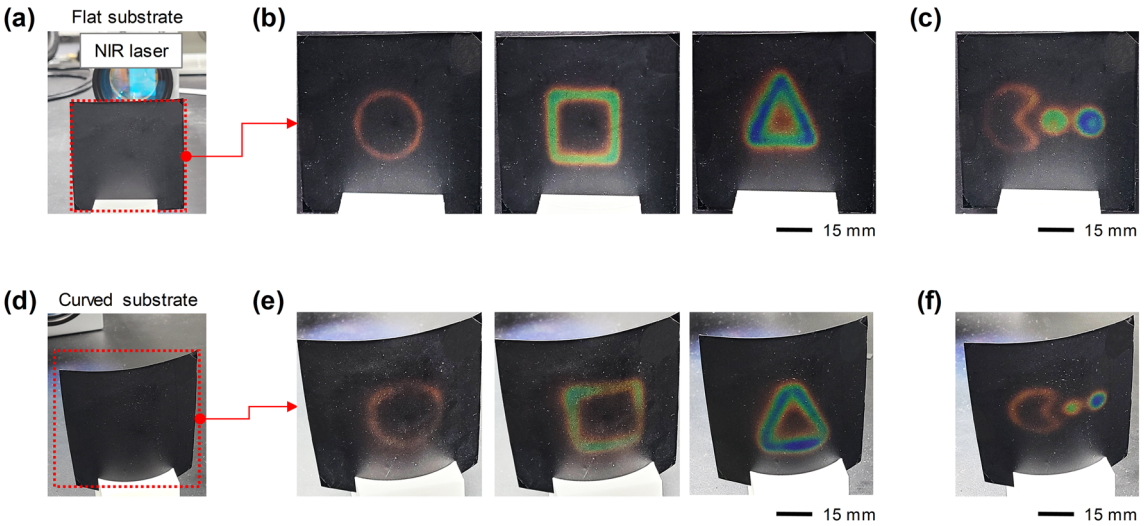

Fig. 5 Images of the light-irradiation-based color-conversion display on flat and curved surfaces. Displays on (a) flat and (d) curved substrates showing (b and e) circular (R), square (G), and triangular (B) images and (c and f) full-color Pac-Man images.

off time used to verify repeatability was fixed at 30/30 s for all the displays. The reliability of the color expression was verified when only the simple condition of the laser power was changed. The color expression was investigated by analyzing the actual display surface temperature using an infrared camera. The corresponding color change was measured using the same camera under the same lighting conditions, and the RGB value changes were extracted and analyzed.

When the laser irradiated the photothermal film, the temperature increased immediately and quickly reached the color-conversion temperature of the TLC; however, the RGB color change had a delay of approximately 5 s, corresponding to the time required for the heat generated by the CNTs to be transferred to the TLC and the helical structure of the material to be transformed. During the thirty laser on/off repetitions, the surface temperature changed and the RGB values remained uniform. When the laser was turned off, the temperature decreased most rapidly when the surface temperature was the highest (blue) because the heat accumulated by the CNTs, which have high thermal conductivity, diffused rapidly and was removed. Thus, the generated heat was quickly transferred to the TLCs and simultaneously diffused outside through the three-dimensional thermal network of CNTs uniformly distributed inside the photothermal film. Additionally, microstructures that could not be identified visually were examined using an optical microscope. Fig. 4(g) shows an image of the TLC capsule after repeated exposure to heat at 40 °C. Heating (40 °C) and cooling (23 °C) were performed repeatedly for 5/5 minutes over 30 cycles. Afterwards, to check for any damage to the TLC caused by heat, the same capsule was tracked and observed. Upon examination of the captured images, no damage from heat was observed, and since the color change due to temperature was maintained, it was confirmed that no abnormalities were present either in the capsule itself or in the TLC inside the capsule.

Fig. 5 shows various images on a light-based color-conversion display with an area of 70 × 70 mm. The desired image was displayed in RGB by controlling the writing conditions of the NIR laser. Fig. 5(a–c) show the images when the display substrate was flat, and Fig. 5(d–f) show the images when the display substrate was fixed to a curved frame. The laser was controlled to show a circle in the color corresponding to the lowest temperature (red, ∼27 °C), a square in the color corresponding to the middle temperature (green, ∼29 °C), and a triangle in the color corresponding to the highest temperature (blue, ∼32 °C). Furthermore, full-color images of Pac-Man were created on the displays. These results confirmed that various shapes and full-color color images could be produced on flat and curved substrates using the simple method of writing with an NIR laser.

Conclusion

In summary, a new type of next-generation display was fabricated that operates using a low-power NIR laser as the driving energy. The substrate was prepared by combining a CNT layer with excellent photothermal and heat dissipation properties and a TLC layer that exhibits full-color changes depending on temperature. The light-irradiation-based color-conversion display fabricated in this study could change from black (<25 °C, initial) to red (27 °C), green (29 °C), and blue (32 °C) by controlling the power (25–56 mW) of the NIR laser and turning it on/off. Considering precise thermal control of ∼2 °C is required to change the color of the TLCs, real-time RGB color implementation and precise color pattern control were implemented using high-efficiency photothermal technology and CNTs that can maintain a uniform temperature distribution. Through free-form laser writing and rapid heat dissipation, images (circles, triangles, squares, and Pac-Man) were generated at the desired positions in red, green, and blue colors. Moreover, desired information was shown on displays with flat and curved surfaces. The fabricated display responded stably to RGB color changes, even after five repeated laser on/off cycles.

Conflicts of interest

The authors declare no completing financial interests.

Data availability

The data that support the findings of this study are available from the corresponding author upon a reasonable request.

Acknowledgements

This work was supported by the National Research Foundation of Korea (NRF) grant funded by the Korea government (MSIT) (RS-2020-NR049541, RS-2022-NR069927, RS-2024-00357747, RS-2024-00358162, and RS-2025-00561597).

References

1 L. Song, X. Yong, P. Zhang, S. Song, K. Chen, H. Yan, T. Sun, Q. Lu, H. Shi, Y. Chen and Y. Huang, *Opt Laser. Technol.*, 2025, **181**, 111710.
2 J.-W. Seo, H. Kim, B. Kim and Y. Kim, *Jpn. J. Appl. Phys.*, 2002, **41**, 7391.
3 P. Leroy, *OLED Microdisplays: Technology and Applications*, 2014, pp. 119–157.
4 G. Li, M.-C. Tseng, Y. Chen, F. S.-Y. Yeung, H. He, Y. Cheng, J. Cai, E. Chen and H.-S. Kwok, *Light: Sci. Appl.*, 2024, **13**, 301.
5 J. Chen, Q. Zhao, B. Yu and U. Lemmer, *Adv. Opt. Mater.*, 2024, **12**, 2300873.
6 P. Li, Y. Wang, X. He, Y. Cui, J. Ouyang, J. Ouyang, Z. He, J. Hu, X. Liu, H. Wei, Y. Wang, X. Lu, Q. Ji, X. Cai, L. Liu, C. Hou, N. Zhou, S. Pan, X. Wang, H. Zhou, C.-W. Qiu, Y.-Q. Lu and G. Tao, *Light: Sci. Appl.*, 2024, **13**, 48.
7 A. B. M. Supian, M. R. M. Asyraf, A. Syamsir, M. I. Najeeb, A. Alhayek, R. N. Al-Dala'ien, G. Manar and A. Atiqah, *Polymers*, 2024, **16**, 1545.
8 A. M. Al-Qahtani, S. Ali, A. Khan and A. Bermak, *Sensors*, 2023, **23**, 1869.
9 P.-A. Blanche, *Photoactive Materials: Synthesis, Applications and Technology*, MDPI, 2021.

10 D. Ge, E. Lee, L. Yang, Y. Cho, M. Li, D. S. Gianola and S. Yang, *Adv. Mater.*, 2015, **27**, 2489–2495.
11 M. N. H. Kashem, K. Gardner, M. R. Momota, B. I. Morshed and W. Li, *Chem. Eng. J.*, 2023, **463**, 142333.
12 J. Van Derlofske, S. Pankratz and E. Franey, *J. Soc. Inf. Disp.*, 2020, **28**, 917–925.
13 N. Abdullah, A. R. Abu Talib, A. A. Jaafar, M. A. Mohd Salleh and W. T. Chong, *Exp. Therm. Fluid Sci.*, 2010, **34**, 1089–1121.
14 T. Jin, Y. Yuan, M. Bagnani, C. Wu, B. Liu and R. Mezzenga, *Adv. Mater.*, 2024, **36**, 2308437.
15 Y. Zhang, H. Liu, J. Niu, X. Wang and D. Wu, *Appl. Energy*, 2020, **264**, 114729.
16 S. L. Levit, J. Nguyen, N. P. Hattrup, B. E. Rabatin, R. Stwodah, C. L. Vasey, M. P. Zeevi, M. Gillard, P. A. D'Angelo, K. W. Swana and C. Tang, *ACS Omega*, 2020, **5**, 7149–7157.
17 W. Zhang, A. P. H. J. Schenning, A. J. J. Kragt, G. Zhou and L. T. de Haan, *ACS Appl. Mater. Interfaces*, 2021, **13**, 3153–3160.
18 Z. Li, A. Lopez-Ortega, A. Aranda-Ramos, J. L. Tajada, J. Sort, C. Nogues, P. Vavassori, J. Nogues and B. Sepulveda, *Small*, 2018, **14**, 1800868.
19 S. Berber, Y.-K. Kwon and D. Tománek, *Phys. Rev. Lett.*, 2000, **84**, 4613–4616.
20 N. W. S. Kam, M. O'Connell, J. A. Wisdom and H. Dai, *Proc. Natl. Acad. Sci. U. S. A.*, 2005, **102**, 11600–11605.
21 D. J. Mulder, A. P. H. J. Schenning and C. W. M. Bastiaansen, *J. Mater. Chem. C*, 2014, **2**, 6695–6705.
22 W. Zhang, A. A. F. Froyen, A. P. H. J. Schenning, G. Zhou, M. G. Debije and L. T. de Haan, *Adv. Photonics Res.*, 2021, **2**, 2100016.
23 P. N. Keating, *Mol. Cryst.*, 1969, **8**, 315–326.
24 Y. Huang, Y. Zhou, C. Doyle and S.-T. Wu, *Opt. Express*, 2006, **14**, 1236–1242.
25 M. Lou, I. Abdalla, M. Zhu, X. Wei, J. Yu, Z. Li and B. Ding, *ACS Appl. Mater. Interfaces*, 2020, **12**, 19965–19973.
26 L. Sangroniz, M. Fernández and A. Santamaria, *Polymer*, 2023, **271**, 125811.
27 A. Jha, P. Karnal and J. Frechette, *Soft Matter*, 2022, **18**, 7579–7592.
28 P. Bernal-Ortega, M. M. Bernal, A. Blume, A. González-Jiménez, P. Posadas, R. Navarro and J. L. Valentín, *Polymers*, 2021, **13**, 821.